

Accepted Manuscript

Uptake of actinides by calcium silicate hydrate (C-S-H) phases

Verena Häußler, Samer Amayri, Aaron Beck, Tim Platte, Tobias A. Stern, Tonya Vitova, Tobias Reich

PII: S0883-2927(18)30238-5

DOI: [10.1016/j.apgeochem.2018.08.021](https://doi.org/10.1016/j.apgeochem.2018.08.021)

Reference: AG 4158

To appear in: *Applied Geochemistry*

Received Date: 29 March 2018

Revised Date: 10 August 2018

Accepted Date: 23 August 2018

Please cite this article as: Häußler, V., Amayri, S., Beck, A., Platte, T., Stern, T.A., Vitova, T., Reich, T., Uptake of actinides by calcium silicate hydrate (C-S-H) phases, *Applied Geochemistry* (2018), doi: 10.1016/j.apgeochem.2018.08.021.

This is a PDF file of an unedited manuscript that has been accepted for publication. As a service to our customers we are providing this early version of the manuscript. The manuscript will undergo copyediting, typesetting, and review of the resulting proof before it is published in its final form. Please note that during the production process errors may be discovered which could affect the content, and all legal disclaimers that apply to the journal pertain.



Uptake of Actinides by Calcium Silicate Hydrate (C-S-H) Phases

Verena Häußler ^a, Samer Amayri ^a, Aaron Beck ^b, Tim Platte ^{a,b}, Tobias A. Stern ^a, Tonya Vitova ^b,
Tobias Reich ^a

^a Johannes Gutenberg University Mainz, Institute of Nuclear Chemistry, Fritz-Strassmann-Weg 2,
55099 Mainz, Germany

^b Institute for Nuclear Waste Disposal, Karlsruhe Institute of Technology, P.O. Box 3640,
76021 Karlsruhe, Germany

verena.haeussler@uni-mainz.de

amayri@uni-mainz.de

aaron.beck@kit.edu

tim.platte@kit.edu

tsstern@students.uni-mainz.de

tonya.vitova@kit.edu

treich@uni-mainz.de

Corresponding author: Tobias Reich

Declarations of interest: none

Abstract

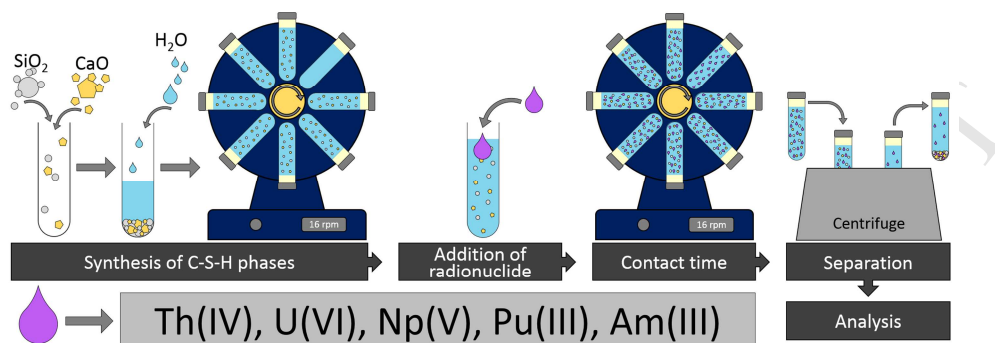
The sorption of actinides (Th, U – Am) was studied in dependence of the solid-to-liquid (*S/L*) ratio (0.5 – 20.0 g/L) and the calcium-to-silicon (C:S) ratio. The C:S ratio was varied between 1.80 and 0.70 to simulate the changing composition of the C-S-H phases during cement degradation from high to low C:S ratios. The decrease of the calcium content in the C-S-H phases by time is accompanied by a decrease in pH in the corresponding suspensions from 12.6 to 10.2. X-ray photoelectron spectroscopy (XPS) of the C-S-H phases showed an increasing depletion of Ca on the surface with increasing C:S ratio in comparison to the composition of the solid phase as a whole.

The sorption experiments were performed with the redox stable species Am(III), Th(IV) and U(VI), as well as the redox sensitive Np(V) and Pu(III). The average distribution coefficients R_d for all investigated actinides are around 10^5 L/kg. The oxidation state of Pu retained by the C-S-H phases was investigated with high-energy resolution X-ray absorption near-edge structure (HR-XANES) spectroscopy. Samples with C:S ratios of 0.75 and 1.65 showed that the initially added Pu(III) was oxidized to Pu(IV) in the course of the experiment.

Keywords

Sorption, radioactive waste, actinides, cement, C-S-H, X-ray photoelectron spectroscopy (XPS), high-energy resolution X-ray absorption near-edge structure (HR-XANES), Th, U, Np, Pu, Am

Graphical abstract



1 Introduction

As in several other countries, the future German repository for high-level nuclear waste will be placed in a deep geological formation. A multi-barrier system, consisting of the host rock as natural barrier and manifold technical barriers, is supposed to enclose the radionuclides for about one million years. Cementitious materials are an important component of the generic repository concepts developed for argillaceous rocks in Northern and Southern Germany (Jobmann and Lommerzheim 2015, Lommerzheim and Jobmann 2015) and consequently can contribute to the retention or the release of the radionuclides.

The main product of cement hydration are C-S-H (calcium silicate hydrate) phases. They basically consist of CaO sheets and short silica chains, exhibit a high specific surface area ($30 \text{ m}^2/\text{g}$ (Pointeau et al. 2001), $148 \text{ m}^2/\text{g}$ (Tits et al. 2014a), $200 - 400 \text{ m}^2/\text{g}$ (Glasser et al. 1987)) and are mainly responsible for the cement's retention capability (Atkins et al. 1992, Gaona et al. 2011). During cement degradation the composition of the C-S-H phases changes, i.e. the molar ratio of calcium to silicon (C:S ratio) decreases and can vary from 1.80 – 0.70 (Chen et al. 2004, Lothenbach and Nonat 2015). This is accompanied by a decrease of the pH (13 – 10) of the solution in equilibrium with cementitious materials.

The nuclear waste, that will be disposed of in a future repository, will contain long-lived actinides, especially neptunium ($t_{1/2} (^{237}\text{Np}) = 2.14 \times 10^6 \text{ a}$) and plutonium ($t_{1/2} (^{239}\text{Pu}) = 2.44 \times 10^4 \text{ a}$), but also

americium and uranium, that make a significant contribution to the waste's long-term radiotoxicity. The actinides can be present in different oxidation states, mainly from +III to +VI. Under the reducing conditions of a repository +III and +IV are dominant and hence investigated in this study. But for a comprehensive study of the sorption behaviour of the actinides on cementitious materials, the oxidation states +V and +VI were included as well. Consequently, with respect to a long-term safety assessment of a repository, it is important to investigate the sorption behaviour of long-lived and radiotoxic nuclides by cementitious materials and C-S-H phases, respectively. Although there is literature data available for the uptake of different trivalent cations on cementitious materials (Ewart et al. 1991, Schlegel et al. 2004, Tits et al. 2003), there has been no investigation on the uptake of Pu(III) by C-S-H phases yet. The uptake of different tetra- (Th(IV), Np(IV) and Pu(IV)), penta- (Np(V)) and hexavalent (Np(VI) and U(VI)) actinides has already been studied and showed a very high uptake by C-S-H phases with just the hexavalent nuclides indicating an influence of the applied C:S ratio on the uptake of actinides (Ewart et al. 1991, Pointeau et al. 2004, Tits et al. 2014a, Tits et al. 2011a, 2014b, Tits et al. 2011b).

In the present study the uptake of the actinides $^{232}\text{Th(IV)}$ (as a redox stable chemical representative, commonly used for tetravalent actinide species) and U – Am ($^{238}\text{U(VI)}$, $^{237}\text{Np(V)}$, $^{239}\text{Pu(III)}$, $^{241}\text{Am(III)}$) on C-S-H phases with different C:S ratios was investigated in order to make a prediction regarding the sorption behaviour of tri-, tetra-, penta- and hexavalent radionuclides with degraded cements in a radioactive waste repository.

2 Materials and Methods

2.1 Materials

All experiments were performed in a glovebox under Ar atmosphere (<0.1 ppm O₂). Solutions were prepared from p.a. quality grade chemicals in MilliQ water (18.2 MΩ, Synergy™ Millipore water system, Millipore GmbH, Schwalbach, Germany) previously degassed with Ar.

2.2 Stock solutions

Stock solutions of 4×10^{-6} M thorium and 4×10^{-5} M uranium were prepared by diluting ICP-MS standard solutions of ^{232}Th (Accu TraceTM, Accu Standard, New Haven, USA) and ^{238}U (Peak Performance, CPI International, Santa Rosa, USA) in 2% HNO_3 , respectively.

For sorption experiments with Np, a ^{239}Np tracer solution, obtained by irradiation of ^{238}U ($\text{UO}_2(\text{NO}_3)_2$ in MilliQ water) and subsequent separation of ^{239}Np from uranium and its fission products on an anion exchange column, was mixed with a $^{237}\text{Np}(\text{V})$ solution in 1 M HClO_4 . The detailed preparation of the ^{239}Np tracer solution is described elsewhere (Amayri et al. 2011).

For the Pu and Am sorption experiments, a 1×10^{-5} M $^{239}\text{Pu}(\text{III})$ solution and a 6×10^{-6} M $^{241}\text{Am}(\text{III})$ solution, each in 1 M HClO_4 , were used. The preparation of the stock solutions is described elsewhere (Amayri et al. 2016).

2.3 Preparation and characterisation of C-S-H phases

Amorphous C-S-H phases with C:S ratios between 0.70 – 1.80 were prepared using the so called “direct reaction” method (Atkins et al. 1992). CaO (Merck, Darmstadt, Germany) and SiO_2 (Aerosil 300, Evonik Industries AG, Essen, Germany) were mixed in MilliQ water to achieve suspensions with solid-to-liquid (*S/L*) ratios between 0.5 and 20.0 g/L. After an aging period of two weeks, during which the samples were rotated in an end-over-end shaker (Stuart Rotator SB3, Stuart, Stone, UK), the C-S-H phases were used in sorption experiments without any phase separation and drying procedure. For sorption experiments with varying C:S ratios, the corresponding *S/L* ratio refers to the weighed amounts of CaO and SiO_2 in the samples, corrected for the Ca and Si concentrations in the supernatant solution. For experiments with varying *S/L* ratios, the dry weight of the solids was determined for each sample.

The specific surface area of the C-S-H phases was determined by N_2 -BET measurements. A detailed description of the measurements and results can be found in the Supplementary Material, section S1. For the C-S-H phases with C:S ratios of 0.75, 1.07 and 1.65 the specific surface areas are $116 \text{ m}^2/\text{g}$, $14 \text{ m}^2/\text{g}$ and $29 \text{ m}^2/\text{g}$, respectively. An estimate for the cation exchange capacity (CEC) of the C-S-H phases was obtained by measuring the uptake of Na^+ in 0.3 M NaOH, using $^{22}\text{Na}^+$ as radioactive tracer,

similar to the work of Hong and Glasser (1999) (see S2 for details). The measured CEC values of the C-S-H phases are 2.56 mol/kg (C:S 0.75), 1.32 mol/kg (C:S 1.07) and 0.45 mol/kg (C:S 1.65).

Furthermore, the C-S-H phases were characterised by X-ray powder diffraction (XRD). The diffractograms show the pattern of C-S-H phases (Garbev et al. 2008, Nonat 2004), whereas the presence of SiO₂ and CaO, i.e. the educts of the synthesis, as well as portlandite, could be excluded (see S3 for details).

2.4 Sorption experiments

All sorption samples were prepared in 10 mL polycarbonate centrifuge tubes (Beckman Coulter, Brea, USA). After the aging period of the C-S-H phases of two weeks, the pH of each suspension was measured and aliquots of the respective actinide stock solution were added. Afterwards the samples were placed again in the end-over-end shaker. The initial actinide concentrations in the suspensions were 1×10^{-8} M for ²³⁹Pu(III), ²⁴¹Am(III), ²³²Th(IV), ^{237/239}Np(V) and 1×10^{-7} M for ²³⁸U(VI), respectively. After a contact time of 72 h, phase separation was carried out by precentrifugation for 5 min at 3770 g (SIGMA 3K30, Sigma Laborzentrifugen GmbH, Osterode, Germany) and further ultracentrifugation for 1 h at 108800 g (Avanti J-301, Beckman-Coulter, Brea, USA). Subsequent removal of the liquid phase and determination of its analyte concentration $[An]_{eq}$ [mol/L] in relation to the initial analyte concentration in the sample $[An]_0$ [mol/L] was used to determine distribution coefficients R_d [L/kg] between the solid and the liquid phases. The sample volume V [L] and the total mass of the solids m [kg] are also taken into account in the R_d calculation.

$$R_d = \frac{V}{m} \cdot \left(\frac{[An]_0 - [An]_{eq}}{[An]_{eq}} \right). \quad (1)$$

2.5 Analytical methods

The concentration of the radionuclides in the liquid phase was analysed by γ -ray spectroscopy for ^{237/239}Np and ²⁴¹Am samples and inductively coupled plasma mass spectroscopy (ICP-MS) for ²³²Th, ²³⁸U and ²³⁹Pu, respectively.

The γ -ray spectroscopy measurements were performed with a HPGe (GMX-13180-S, EG & G ORTEC) coaxial γ -ray detector, Canberra InSpector 2000 (model IN2K, Canberra Industries, Inc., USA), in combination with the Genie 2000 Gamma acquisition and analysis software (Canberra Industries, Inc., USA). The calibration of the spectroscopic system was performed with the mixed radionuclide γ -ray standard reference solution QCY48 (No: 1921-6, Eckert und Ziegler, Berlin, Germany). The resulting limits of detection (LOD) are 3×10^{-16} mol/L for ^{239}Np and 1×10^{-11} mol/L for ^{241}Am , respectively.

ICP-MS measurements were performed with a 7500ce Series ICP-MS (Agilent Technologies, Santa Clara, USA). Prior to ICP-MS analysis, all samples were acidified with concentrated HNO_3 . Aliquots of ^{193}Ir in 2% HNO_3 were added as internal standard ($c(\text{Ir}) = 200$ ppt). The LOD for ICP-MS measurements of ^{232}Th , ^{238}U and ^{239}Pu were 3×10^{-11} mol/L, 1×10^{-11} mol/L and 2×10^{-11} mol/L, respectively. Beside the determination of the radionuclide concentration in the samples, further ICP-MS measurements were performed to determine the Ca (LOD: $c(\text{Ca}) = 3 \times 10^{-6}$ mol/L) and Si (LOD: $c(\text{Si}) = 6 \times 10^{-8}$ mol/L) concentrations in the C-S-H supernatant solution. For the Si measurements the H_2 reaction mode was used.

The pH was determined using a pH meter (WTW ino Lab. pH Level 1, WTW GmbH, Weilheim, Germany) equipped with a temperature sensor (WTW TFK 150) and a BlueLine 16 pH electrode (Schott Instruments GmbH, Mainz, Germany). The pH meter had to be calibrated with the certified commercial DIN buffers at pH = 4.01, 6.87 and 9.18 (Schott Instruments, Mainz, Germany). As pH values above this calibration range were measured in the experiments, a certified DIN buffer at pH 13.00 (Hanna Instruments, Inc., Woonsocket, USA) was measured, using this calibration. The resulting pH value was 12.89, giving an error of $\Delta\text{pH} = 0.11$. The redox potential was measured with a BlueLine 31 Rx electrode (Schott Instruments, Mainz, Germany). The electrode was checked with a standard solution with a redox potential of +220 mV (Schott Instruments, Mainz, Germany).

The C-S-H phases were further analysed with X-ray photoelectron spectroscopy (XPS) to determine the solids' surface composition. For this, the dried C-S-H powders (drying occurred under Ar atmosphere at room temperature for at least 72 h) were milled in an agate mortar and a small amount was pressed into an indium foil on a copper sample holder. The measurements were performed at

room temperature under a vacuum of 7×10^{-9} mbar with a custom-built XPS system (SPECS GmbH, Berlin, Germany). For photoelectron excitation, the non-monochromatic MgK_α radiation (1253.6 eV) from a high-intensity twin anode (Al/Mg) X-ray source XR-50 was used. Photoelectron detection was performed with a constant analyser pass energy of 13 eV using the hemispherical energy analyser PHOIBOS 100. The spectra were analysed with CasaXPS (version 2.3.15). The energy calibration was performed using the C1s signal of adventitious hydrocarbons (285.0 eV).

2.6 *High-energy resolution X-ray absorption near-edge structure (HR-XANES) spectroscopy*

As Pu is very redox sensitive, its oxidation state could change during the course of a sorption experiment. To determine the oxidation state of the sorbed Pu species, Pu M_5 -edge HR-XANES spectroscopy was applied on sorption samples which were prepared in 10 mL polycarbonate centrifuge tubes (Beckman Coulter, Brea, USA) with a S/L ratio of 2.5 g/L. The used C-S-H phases exhibited C:S ratios of 0.75 and 1.65. After an aging period of two weeks, aliquots of the $^{239}\text{Pu(III)}$ stock solution were added to achieve an initial Pu concentration of 1×10^{-5} mol/L in the samples. After a contact time of 72 h, meanwhile the samples were placed in an end-over-end shaker and the pH was regularly controlled, the phases were separated by precentrifugation and ultracentrifugation as described in section 2.4. Afterwards the liquid phase was removed and its pH and Eh were measured. The wet C-S-H phases were allowed to dry at room temperature under Ar atmosphere for several days. Subsequently, the dried solids were milled and placed in an aluminium sample holder with double containment and Kapton® foil (ADVENT Research Materials Ltd, Oxford, UK) exit windows. The inner and outer containments were equipped with 8 μm and 12.5 μm Kapton® foils, respectively. The measurements of the samples were performed at the CAT-ACT-Beamline, Karlsruhe Research Accelerator (KARA) (Karlsruhe, Germany), at room temperature. A detailed description of this beamline and its components can be found elsewhere (Bahl et al. 2017, Vitova et al. 2017, Zimina et al. 2017, Zimina et al. 2016). The primary beam was collimated by a bare Si cylindrically bent mirror, monochromatized by a Si(111) double crystal monochromator (DCM) and focused to $500 \times 500 \mu\text{m}^2$ into the sample by a toroidal Si mirror. A slit with $500 \times 500 \mu\text{m}^2$ size was placed at about 20 cm from

the sample. The HR-XANES spectra were measured with a Johann type X-ray emission spectrometer with 1 m Rowland circle diameter. The spectrometer comprises five spherically bent Si(220) analyzer crystals (Saint-Gobain Crystals, Nemours, France), which diffracted and focused the Pu M_{α} characteristic fluorescence (3339 eV) on a single diode VITUS Silicon Drift Detector (KETEK, München, Germany). The crystals were aligned at 75.22° Bragg angle. The HR-XANES spectra were obtained by recording the maximum intensity of the Pu M_{α} emission line as a function of the incident photon energy. The X-ray emission spectrometer was placed in a He-filled box in order to minimize the absorption/scattering of the tender X-ray photons (Zimina et al. 2017, Zimina et al. 2016).

An integration time of 1 s/step for the PuO₂ reference and 20 s/step for the sample, and varying step sizes (3760–3770 eV: 0.5 eV; 3770–3790 eV: 0.1 eV; 3790–3835 eV: 0.5 eV) were used to execute the measurement. For each sample three scans were averaged. The PuO₂ reference was measured before and after the measurement of each sample. Background subtraction and energy calibration of the spectra were performed using the software package ATHENA (Demeter 0.9.25) (Ravel and Newville 2005). The maximum of the most intense absorption peak (white line) of the Pu M_5 edge of the PuO₂ reference was calibrated to 3775.0 eV.

3 Results and discussion

3.1 C-S-H phases

The pH of C-S-H suspensions depends on their composition and decreases with decreasing C:S ratio (Figure 1).

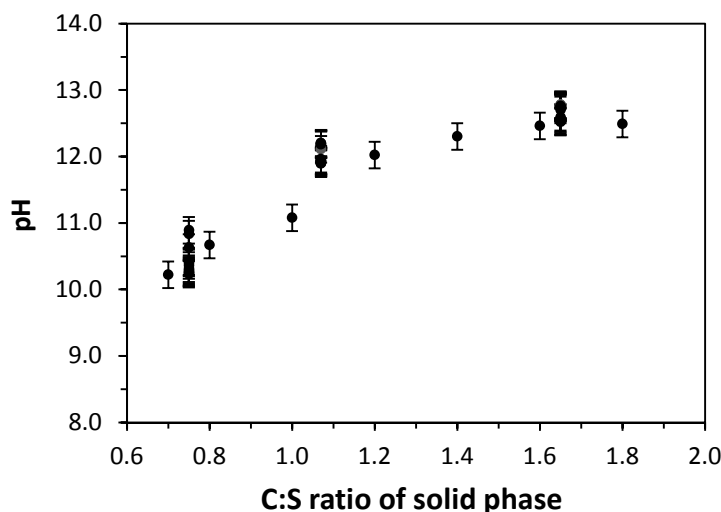


Figure 1: Measured pH values in C-S-H suspensions (0.5 – 20.0 g/L) in MilliQ water after two weeks of synthesis of C-S-H phases with different C:S ratios.

After two weeks of synthesis of the C-S-H phases, the resulting pH values of the suspensions were between 10.2 and 12.5 for solids with C:S ratios of 0.7 and 1.8, respectively. This is in good agreement with literature data (Gaona et al. 2013, Lothenbach and Nonat 2015, Tits et al. 2014b).

The supernatant solution of different C-S-H suspensions in MilliQ water was analysed by ICP-MS to determine the Ca and Si content in the supernatant ($c_{sol.}(Ca/Si)$). For this purpose, samples with $V = 40$ mL and $S/L = 15.0$ g/L were prepared.

The investigated suspensions contained C-S-H phases with C:S target ratios of 0.75, 1.07 and 1.65. As shown in Figure 2, the determined Ca and Si concentrations in solution match well with literature data (Schlegel et al. 2004, Tits et al. 2011a, Tits et al. 2006). Based on the measured pH values, the Ca and Si concentrations and the XRD data (S3), we conclude that the preparation of the C-S-H phases using the “direct reaction” method was successful.

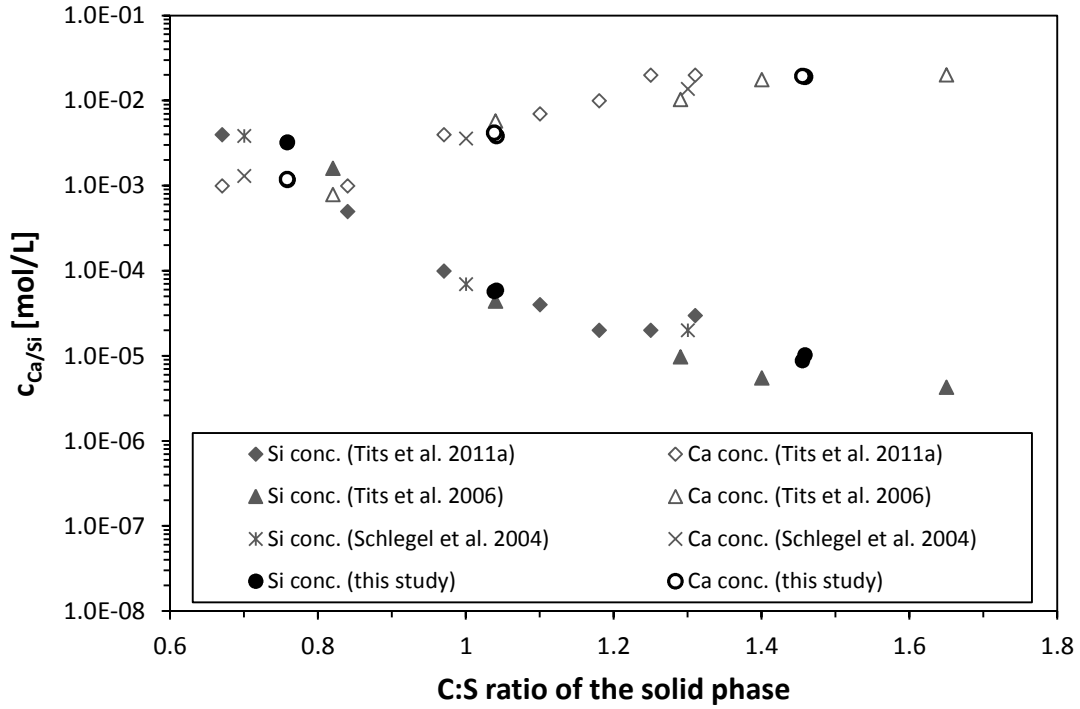


Figure 2: Composition of the aqueous solution after equilibration with C-S-H phases with different C:S ratios in MilliQ water (S/L = 15 g/L) determined by ICP-MS and comparison to literature data.

The C:S ratio of the solid can be deduced from the Ca and Si content in the supernatant ($c_{sol.}(Ca/Si)$) and the initially applied amounts of Ca and Si ($n_i(Ca/Si)$) using equation (2).

$$C:S = \frac{n_i(Ca) - c_{sol.}(Ca) \cdot V}{n_i(Si) - c_{sol.}(Si) \cdot V} \quad (2)$$

For ICP-MS the samples with C:S target ratios of 0.75, 1.07 and 1.65 were prepared and analysed in duplicate. In Table 1 the average measured concentrations of Ca and Si in the supernatants as well as the derived C:S ratios are listed. For the sample with C:S 0.75 the determined ratio fits well with its target value. With increasing C:S ratio the divergence with the target values increases.

Table 1: Concentration of calcium and silicon in the supernatant solution of C-S-H phases with S/L = 15.0 g/L and V = 40 mL determined by ICP-MS measurements and calculated C:S ratio.

C:S target ratio	$n_i(\text{Ca})^*$ [mol]	$n_i(\text{Si})^*$ [mol]	$c_{sol.}(\text{Ca})$ [mol/L]	$c_{sol.}(\text{Si})$ [mol/L]	calculated C:S ratio of the solid phase
0.75	4.41×10^{-3}	5.87×10^{-3}	$(1.2 \pm 0.2) \times 10^{-3}$	$(3.2 \pm 1.0) \times 10^{-3}$	0.76
1.07	5.35×10^{-3}	5.00×10^{-3}	$(4.0 \pm 0.2) \times 10^{-3}$	$(5.8 \pm 1.9) \times 10^{-3}$	1.04
1.65	6.49×10^{-3}	3.93×10^{-3}	$(1.9 \pm 0.1) \times 10^{-2}$	$(9.6 \pm 3.5) \times 10^{-6}$	1.46

* Moles used in synthesis

XPS measurements were used for further analysis of the C-S-H phases' surfaces. Samples with C:S ratios of 0.70, 0.75, 1.20 and 1.80 were investigated. The received spectra showed oxygen, calcium and silicon signals, that were analysed using equation (3) on the basis of the O1s, Ca2p and Si2p intensities, respectively. For the calculation of a particular atomic ratio (n_a/n_b) from the XPS spectrum, the intensity of the relevant signal I_{ab} was used with regard to the corresponding photoionization cross section σ_{ab} . In this calculation the cross sections were combined in an empirically determined sensitivity factor $S_{Si/Ca} = 0.19$.

$$\frac{n_{\text{Ca}}}{n_{\text{Si}}} = \frac{I_{\text{Ca } 2p}}{I_{\text{Si } 2p}} \cdot S_{\text{Si/Ca}} \quad (3)$$

The comparison of the C:S ratios applied in the synthesis of the C-S-H phases with the results from the XPS measurements shows significant discrepancies for all samples (Table 2). The values determined by XPS are collectively lower than their target values and the differences become higher with increasing C:S ratio. In general, the same trend can be seen in literature data (Tits et al. 2006) where the analysis of the C-S-H phases was performed by acid decomposition of the solids with HF and analysis of the resulting solutions with ICP-OES, which allows the determination of the bulk composition of the investigated phases. However, the thus determined C:S ratios, as well as the C:S ratios determined by ICP-MS analysis of the solution, fit as a whole better with their targeted values than those obtained from XPS measurements for which the milled solid was directly used without further treatment and analysis was performed for the surface of the sample. Considering the C:S ratios determined by XPS, the C-S-H surface seems to be more depleted of Ca than the solid as a whole for all samples, though the depletion effect increases with increasing C:S ratio.

Table 2: C:S target ratios in comparison to the C:S ratios determined by XPS measurements (the estimated errors are about $\pm 10\%$) and literature data.

C:S target ratio	0.70	0.75	1.20	1.80
C:S ratio (XPS)	0.63	0.70	0.98	1.25
C:S (Tits et al. 2006) bulk analysis (ICP-OES)	-	0.82	-	1.65*

* For a C:S target ratio of 1.82

3.2 Sorption experiments

The uptake of the different actinides by C-S-H phases was determined in dependence of the applied *S/L* ratio and the C:S ratio of the solid. For all sorption experiments a contact time of 72 h was chosen on the basis of the available literature data for the sorption kinetics of Eu(III) (Pointeau et al. 2001, Schlegel et al. 2004), Th(IV) (Tits et al. 2014a) and Np(V) (Tits et al. 2014b) on C-S-H phases. All these experiments showed a fast sorption kinetics with a steady state reached within the first two days or even faster. Tits et al. (2011a) observed a fast sorption kinetics with sorption equilibrium reached within less than three days for Th(IV), U(VI) and Np(IV/V/VI). However, for U(VI) also longer equilibration times of 9 – 10 d were reported (Pointeau et al. 2004, Tits et al. 2014a, Tits et al. 2011b). But regarding the almost quantitative uptake that was observed in our experiments after 72 h, this contact time appears to be quite reasonable, even for U(VI).

Furthermore, the actinide uptake was investigated at one initial actinide concentration (except for the Pu HR-XANES experiments), which was chosen for every actinide with regard to its solubility limit, that had to be undercut at least by the equilibrium concentration in the experiment, and the LOD of the used analytical method.

The uptake of actinides in different oxidation states by C-S-H phases was determined for *S/L* ratios between 0.5 – 20.0 g/L. To cover all relevant actinide oxidation states, these experiments were performed for 1×10^{-8} M Am(III), Th(IV), Np(V) and 1×10^{-7} M U(VI). As shown in Figure 3, the resulting average distribution coefficients $R_d(av)$ are $\sim 10^5$ L/kg (min.: 3×10^4 L/kg, max.: 1×10^6 L/kg). Although the R_d values vary over two orders of magnitude, the actinide uptake is about 98% or even higher in all samples. With regard to the resulting low analyte concentration in the samples' supernatant and the corresponding high errors in quantification, resulting in an uncertainty of

about 50% for the determined R_d values, the S/L ratio in the considered range seems to have no influence on the actinide uptake in the oxidation states from +III to +VI. In Figure 3 the data for sorption experiments for Am(III), Th(IV) and U(VI) with C:S 0.75 and for Np(V) with C:S 1.07 are shown. Additional experiments (not shown here), that were performed with Am(III), Np(V) and U(VI) with C:S 0.75 – 1.65, showed R_d values in the same range as those given in Figure 3.

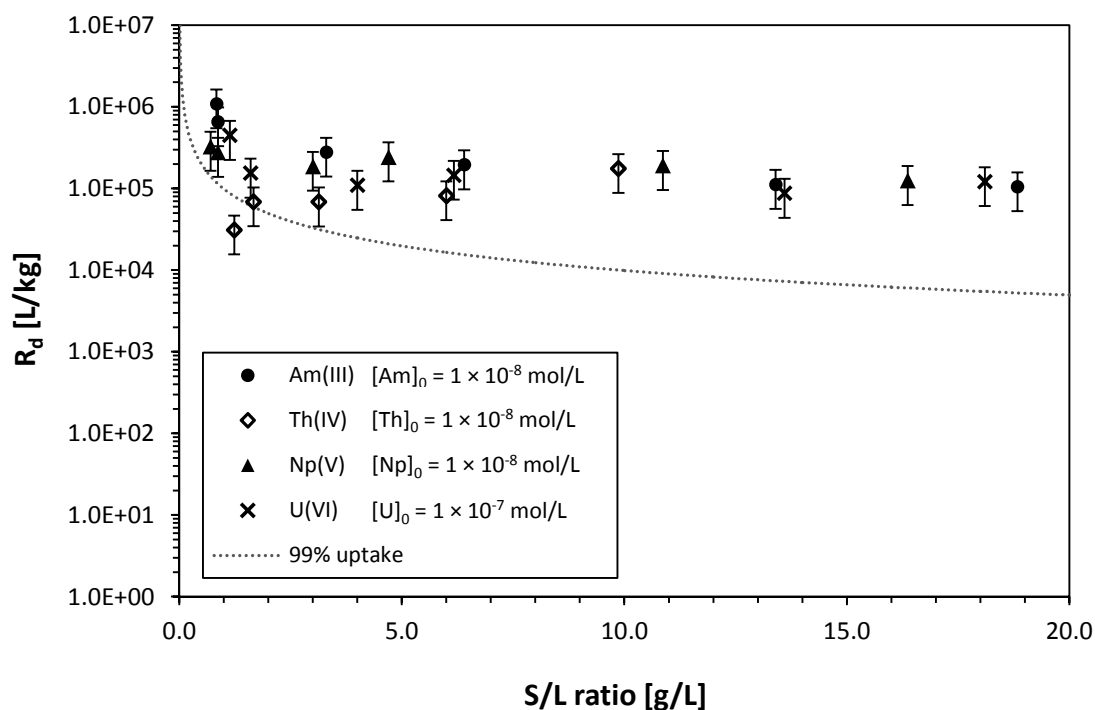


Figure 3: Distribution coefficients R_d for the sorption of Am(III), Th(IV), Np(V) and U(VI) on C-S-H phases with C:S 0.75 (C:S 1.07 for Np(V)) in MilliQ water as a function of S/L ratios between 0.7 – 19.0 g/L. The dotted line corresponds to R_d values calculated for an actinide uptake of 99%.

The safety assessment of a nuclear waste repository should consider an early release of radionuclides in a surrounding characterized by fresh cement (high C:S ratios of ~ 1.80), as well as the release into degraded cement (low C:S ratios of ~ 0.75) after a long-term enclosure. Therefore, it is important to investigate the influence of the C:S ratio on the radionuclide uptake by C-S-H phases. For the sorption experiments with varying C:S ratios, a S/L ratio of 5.0 g/L was applied. All samples, independent of the containing radionuclide and its oxidation state, showed an uptake of $\geq 99\%$ of the initial radionuclide content, resulting in high R_d values from 2×10^4 to 9×10^5 L/kg (Figure 4).

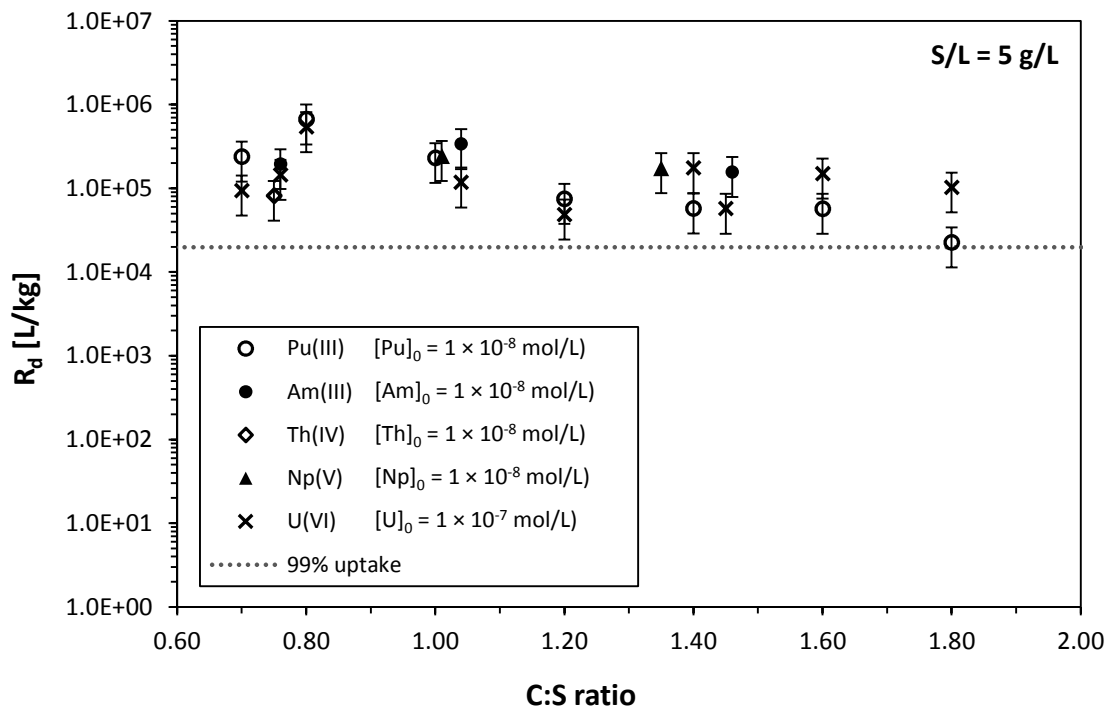


Figure 4: Distribution coefficients R_d for the sorption of Pu(III), Am(III), Th(IV), Np(V) and U(VI) on C-S-H phases in MilliQ water for $S/L = 5.0$ g/L and C:S ratios between 0.7 – 1.8. The dotted line corresponds to R_d values calculated for an actinide uptake of 99%.

In the following section, the determined R_d values for the different actinides and oxidation states are discussed starting with their redox stable representatives Am(III), Th(IV) and U(VI) and continuing to the redox sensitive actinides Np(V) and Pu(III). A summary of the measured R_d values and a comparison with the available literature data is shown in Table 4.

The investigations of the uptake of trivalent actinides/lanthanides by C-S-H phases reported in the literature obtained R_d values between 2.7×10^4 L/kg and 6×10^5 L/kg. The distribution coefficients for Am(III) determined in this study ($R_d(av) = 4 \times 10^5$ L/kg) support the data already known from literature. Speciation calculations with PHREEQC (version 3.3.5, (Parkhurst and Appelo 2016)) using the PSI database (Nagra 12/07, (Thoenen et al. 2014)) predict $\text{Am}(\text{OH})_2^+$ and with further increasing pH $\text{Am}(\text{OH})_3(\text{aq})$ as the dominating species in solution under the considered conditions. Here as well as in the following speciation calculations, the Ca and the Si concentrations in the supernatant solution were always taken into account, but had just an influence on the formation of minor species at high pH values. The strong sorption of Am(III) can be rationalized in part by the electrostatic interaction of

$\text{Am}(\text{OH})_2^+$ with the negatively charged C-S-H surface. But this does not explain the strong sorption at higher pH values with $\text{Am}(\text{OH})_3(\text{aq})$ becoming the dominant species.

In general, the strong sorption can be explained through the formation of surface complexes with silanol groups of the C-S-H phases (Pointeau et al. 2004, Tits et al. 2011a, Tits et al. 2011b). The strength of this surface complexation should decrease together with the effective charge of the actinides according to An^{4+} (4) > AnO_2^{2+} (3.3) > An^{3+} (3) > AnO_2^+ (2.2) (Tits et al. 2014b). However, the measured R_d values are similar for all oxidation states and independent of the effective charge of the actinide. Similar R_d values for the sorption of Np(IV), Np(V) and Np(VI) on C-S-H at pH 10 were rationalized using the concept of inter-ligand electrostatic repulsion between hydroxyl groups in the Np coordination sphere (Tits et al. 2014b). This concept was introduced to predict the complexation constants of actinides with inorganic ligands in aqueous solution (Fanghänel and Neck 2002, Neck and Kim 2000, 2001). According to this concept the actinide (An) species $\text{An}(\text{III})(\text{OH})_3(\text{aq})$, $\text{An}(\text{IV})(\text{OH})_4(\text{aq})$, $\text{An}(\text{V})\text{O}_2\text{OH}(\text{aq})$ and $\text{An}(\text{VI})\text{O}_2(\text{OH})_3^-$ can add one more hydroxyl ligand to their coordination sphere, whereas this is impossible for $\text{An}(\text{VI})\text{O}_2(\text{OH})_4^{2-}$ and $\text{An}(\text{V})\text{O}_2(\text{OH})_2^-$. The former are then able to form a surface complex with a silanol group of the C-S-H phase as an additional ligand (Fanghänel and Neck 2002, Tits et al. 2014b). Therefore, the strong sorption of Am(III) on C-S-H at high pH values can be explained qualitatively by the capability of the $\text{Am}(\text{OH})_3(\text{aq})$ species to form a surface complex with the silanol groups of the C-S-H phases.

Distribution coefficients for tetravalent actinides on C-S-H phases are also available in literature and fit well to the data obtained in this study with $R_d(\text{av}) = 2 \times 10^5$ L/kg for Th(IV). The related speciation calculations show that $\text{Th}(\text{OH})_4(\text{aq})$ is the only solution species that interacts with the C-S-H phases in the considered pH range. As well as for Am(III), the strong sorption can be explained by the concept of inter-ligand electrostatic repulsion which allows a $\text{An}^{\text{IV}}(\text{OH})_4(\text{aq})$ species to add one more ligand, namely a surface silanol group, to its coordination sphere.

Speciation calculations for U(VI) indicate the negatively charged species $\text{UO}_2(\text{OH})_3^-$ and $\text{UO}_2(\text{OH})_4^{2-}$ to be present under the considered conditions (Figure 5). Particularly $\text{UO}_2(\text{OH})_4^{2-}$, which becomes the dominating species with increasing pH, could be repelled by the negatively charged

surface of the C-S-H phases under alkaline conditions. This would imply a decreasing distribution coefficient with increasing C:S ratio and pH, respectively, as described in the literature. Also the concept of inter-ligand electrostatic repulsion would predict a strong sorption through surface complexation for $\text{UO}_2(\text{OH})_3^-$, but not for $\text{UO}_2(\text{OH})_4^{2-}$. For hexavalent actinides Tits et al. (2014b), Tits et al. (2011a), Tits et al. (2011b) and Pointeau et al. (2004) found decreasing R_d values with increasing C:S ratio, i.e. with increasing pH. Although the distribution coefficients for U(VI) are still in the range of the data for actinides in the +III, +IV and +V oxidation states, the R_d values show a slightly negative slope with increasing C:S ratio. In addition, all R_d values for Np(VI) are lower than those for other oxidation states and also as for U(VI). They show a negative slope with increasing C:S ratio as well. Since we did not study the sorption of Np(VI), only the data for U(VI) can be compared. The decrease of the published R_d values embraces about one order of magnitude. Considering the error range of the data points, resulting from the low analyte concentration in solution after phase separation, the data shown in Figure 4 do not indicate a decrease of the distribution coefficients with increasing C:S ratio under the experimental conditions of this study. The determined $R_d(av)$ value is 1×10^5 L/kg. The large experimental uncertainty could be the reason that the moderate decrease of the R_d values reported by others was not observed in this study.

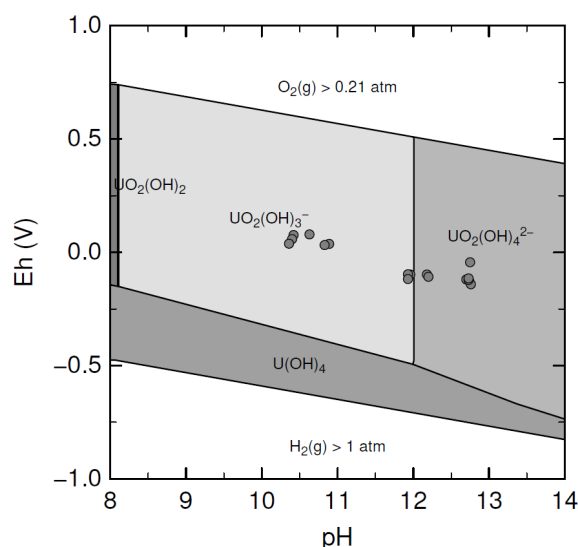


Figure 5: Predominance diagram for an equilibrium concentration of $1 \times 10^{-9} \text{ M U(VI)}$ in the system C-S-H/MilliQ water for C:S ratios of 0.75, 1.07 and 1.65. The grey dots mark the measured Eh and pH values of the sorption samples. (Graphic generated by PhreePlot (version 1.0, (Kinniburgh and Cooper 2011)) using PHREEQC and the PSI database (Nagra 12/07)).

As Np(V) is redox sensitive in comparison to the previously discussed species, Eh measurements were performed for all Np samples to assess the actinides oxidation state after the sorption process. For a low C:S ratio the Eh values are within the stability range of Np(V), for higher C:S ratios they are on the border between Np(V) and Np(IV) (Figure 6). The speciation of Np(V) changes from NpO_2^+ to $NpO_2(OH)(aq)$ and further on to $NpO_2(OH)_2^-$ with increasing pH. It should be noted that a large error range for the Eh measurements has to be taken into account, because of the low residual Np concentration in the solution after phase separation (Gaona et al. 2013), meaning that the redox potential is not controlled by the corresponding Np redox couple, but possibly by any other redox couple present in the sample as impurity, e.g. traces of oxygen. Therefore, we consider the Eh measurements as inconclusive concerning the actual oxidation state of Np.

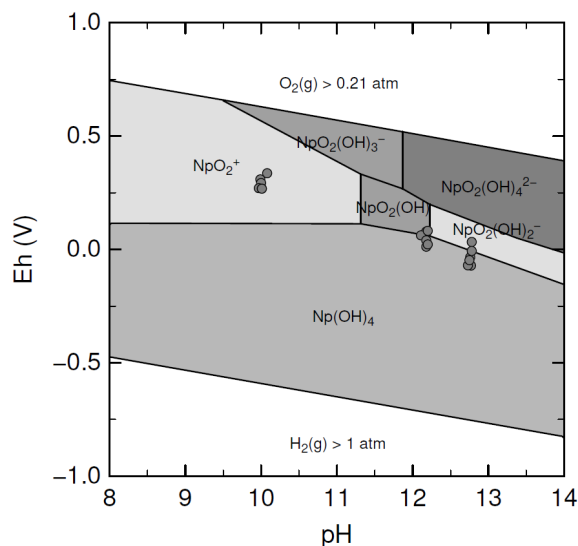


Figure 6: Predominance diagram for an equilibrium concentration of 1×10^{-10} M Np(V) in the system C-S-H/ MilliQ water for C:S ratios between 0.75 – 1.65. The grey dots mark the measured Eh and pH values of sorption samples with different C:S ratios. (Graphics generated by PhreePlot (version 1.0, (Kinniburgh and Cooper 2011)) using PHREEQC and the PSI database (Nagra 12/07)).

To ascertain the actual Np oxidation state after sorption on C-S-H phases in MilliQ water under alkaline conditions, Gaona et al. investigated a Np(V) sample by EXAFS measurements and could exclude the formation of Np(IV) due to the identification of equatorial as well as axial (being related to the linear neptunyl unit) coordinated oxygen atoms (Gaona et al. 2013). Considering this study and its experimental conditions (C:S ratios 0.75, 1.07 and 1.65, $S/L = 2.5$ g/L, $c(Np) = 9.8 \times 10^{-5}$ M) the Np oxidation state in our experiments should be +V as well.

For Np(V) distribution coefficients for the sorption on C-S-H phases are also available in literature and fit well to the results from this study with $R_d(av) = 5 \times 10^5$ L/kg.

For the redox sensitive species Pu(III) no distribution coefficients are available in literature, but values of $R_d(av) = 2 \times 10^5$ L/kg fit well with the available Eu(III) and Am(III) data. Also the speciation calculations predict similar aqueous species as for Am(III), i.e. $Pu(OH)_2^+$ (Figure 7). Although the measured R_d values for Pu agree with the values expected for Pu(III), the initial oxidation state in the experiment, the redox sensibility of Pu requires further considerations. For this reason, Eh and pH measurements of the supernatant solutions were performed. As for Np, a large error range of at least ± 0.05 V for the Eh measurements has to be taken into account, due to the low concentration of the

concerning redox couple. Nevertheless, the determined Eh values indicate that Pu(III) should be oxidized to Pu(IV) during the batch experiment (Figure 7). In addition, the calculation predicts the formation of $\text{PuO}_2(\text{hyd,aged})$ at the equilibrium concentration of 1×10^{-10} M Pu(IV). Therefore, precipitation of Pu(IV) can contribute to the measured R_d values for the uptake of Pu by C-S-H phases.

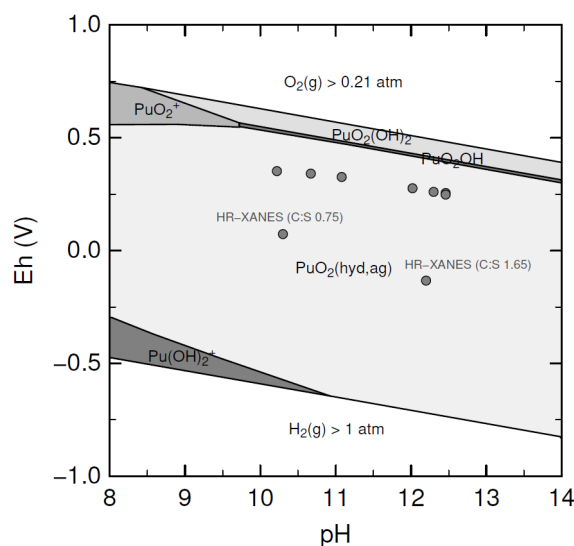


Figure 7: Predominance diagram for an equilibrium concentration of 1×10^{-10} M Pu(III) in the system C-S-H/ MilliQ water for C:S ratios between 0.7 – 1.8. The grey dots mark the measured Eh and pH values of the sorption samples with different C:S ratios and the samples for HR-XANES with C:S 0.75 and 1.65. (Graphics generated by PhreePlot (version 1.0, (Kinniburgh and Cooper 2011)) using PHREEQC and the PSI database (Nagra 12/07)).

For more information about the Pu oxidation state at the C-S-H surface, further investigations were performed with Pu M_5 -edge HR-XANES for samples with higher Pu concentrations. The initial concentration of 1×10^{-5} M Pu(III) was necessary to make this spectroscopic investigation feasible. It should be noted that at an equilibrium concentration of 1×10^{-7} M, the C-S-H suspensions were oversaturated with respect to $\text{PuO}_2(\text{hyd,aged})$.

The Pu M_5 -edge HR-XANES spectrum measures the dipole-allowed transitions of $3d_{5/2}$ electrons to $5f$ unoccupied states (Bahl et al. 2017). The Pu M_5 -edge HR-XANES spectrum shifts to higher energies from Pu(III) over Pu(IV) to Pu(VI) (Bahl et al. 2017). The energies of the white lines of the Pu(III)^{3+} , Pu(IV)O_2 and Pu(VI)O_2^{2+} spectra reported in Vitova et al. (2017) and Bahl et al. (2017) as well as the energies for the measured samples are listed in Table 3. The Pu M_5 -edge HR-XANES spectra for the Pu/C-S-H samples and the Pu(IV)O_2 reference are shown in Figure 8.

Table 3: Peak maxima for the Pu(III)³⁺, Pu(IV)O₂ and Pu(VI)O₂²⁺ oxidation state references (white line and post edge feature) (Bahl et al. 2017) and for the studied samples.

White line of Pu M ₅ -edge HR-XANES	Energy / eV
Pu(III) ³⁺	3774.1*
Pu(IV)O ₂	3775.0*
Pu(VI)O ₂ ²⁺	3776.2*
Post edge feature of Pu(VI)O ₂ ²⁺	3780.5*
Pu/C-S-H sample (C:S 0.75)	3775.4*
Pu/C-S-H sample (C:S 1.65)	3775.2*

* The spectra are measured without slit in front of the sample.

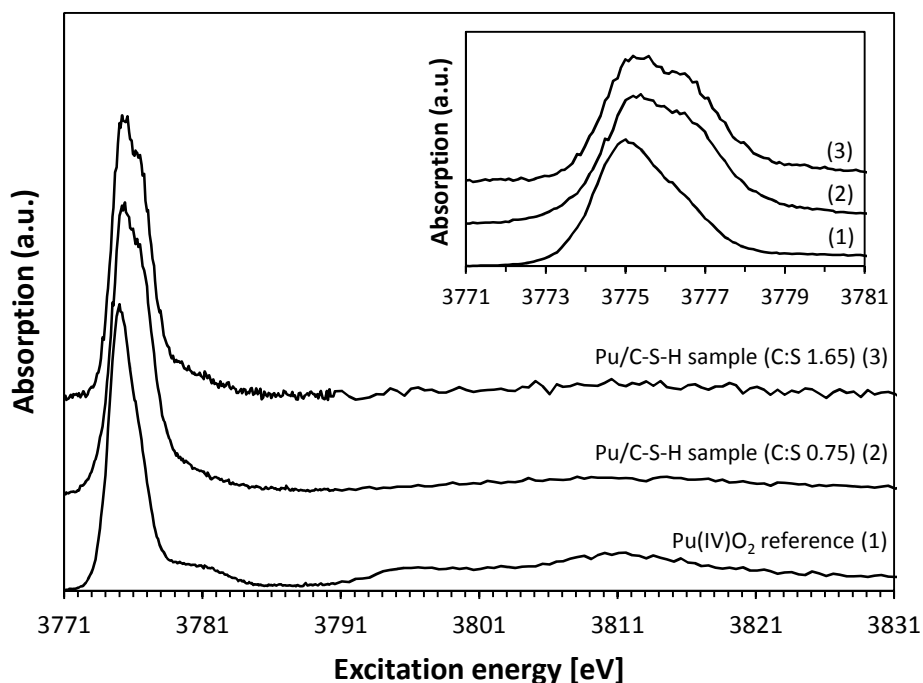


Figure 8: Pu M₅ edge HR-XANES spectra of the Pu/C-S-H samples with C:S 0.75 and C:S 1.65 and the corresponding Pu(IV)O₂ reference.

The spectrum of Pu(VI)O₂²⁺ (plutonyl) has a characteristic second peak at about 3780.5 eV (Vitova et al. 2015, Vitova et al. 2017). A similar peak but at 2 – 3 eV lower energy is expected for Pu(V)O₂⁺. These features describe transitions to the sigma antibonding (σ^*) molecular orbital and are also typical for the spectra of U(V)/U(VI)-yl (Podkovyrina et al. 2016, Vitova et al. 2015). Note that, as discussed in Vitova et al. (2017), the energy positions of the spectral peaks can slightly depend on the energy resolution of the experimental set-up. We exclude the formation of Pu(V)O₂⁺/Pu(VI)O₂²⁺ in our samples since such characteristic peaks are not present in the spectra.

In order to decide whether the plutonium taken up by the C-S-H phases is Pu(III) or Pu(IV), the positions of the white lines of the spectra for the samples and the PuO₂ reference are compared. The white lines of both sample spectra are slightly shifted to higher energies ($\Delta E = 0.2 - 0.4$ eV). Regarding a previous study of Pu, the white line for Pu(III) should be shifted about 1 eV to lower energies compared to the PuO₂ reference (Bahl et al. 2017). Therefore, it can be assumed that Pu(IV) is the dominant species on the surface of the C-S-H-phases in both samples. The oxidation of Pu appears to be independent of the applied C:S ratio of the C-S-H phases during the course of the experiment since the two spectra of the samples are very similar. Furthermore, the shoulder on the high energy side of the white line might indicate a contribution of a second Pu species like for example Pu(V) (plutonate) or a different bonding partner of Pu(IV) as OH/OH₂. It has been recently shown that the U M₄-edge HR-XANES method is very sensitive and can detect U(IV), U(V) and U(VI) when mixed and in small amounts sorbed onto or incorporated in magnetite (Pidchenko et al. 2017). For final clarification further measurements of various reference samples are required. The post-edge region of the Pu/C-S-H spectra exhibits one broad peak and does not resemble the double structure of the post-edge region of the Pu(IV)O₂ reference spectrum. The post-edge region of the spectrum of Pu dispersed in borosilicate glass reported in Bahl et al. (2017) has a similar broad single structure and indicates that Pu does not form any ordered crystalline phases on the surface of C-S-H. The results of HR-XANES spectroscopy are consistent with the conclusions drawn from the predominance diagram (Figure 7).

Table 4: Comparison of the results of this study (average distribution coefficients $R_d(av)$ for all samples of one species independent of S/L and C:S ratio) with available literature data for distribution coefficients of different metal cations in the oxidation states from +III to +VI.

M³⁺			
Species	Initial analyte concentration c_i [mol/L]	Distribution coefficient R_d [L/kg]	source
Eu(III)	1×10^{-4}	$\geq 2.7 \times 10^4$	(Pointeau et al. 2001)
	2.6×10^{-10}	$\geq 1.8 \times 10^5$	
Am(III)	2×10^{-9}	$(6 \pm 3) \times 10^5$	(Tits et al. 2003)
	1×10^{-11}	$(6 \pm 2) \times 10^4$	(Ewart et al. 1991)
	1×10^{-8}	4×10^5	(This study)
M⁴⁺			
Species	Initial analyte concentration c_i [mol/L]	Distribution coefficient R_d [L/kg]	source
Th(IV)	1×10^{-8}	2×10^5	(This study)
Np(IV)	1.5×10^{-10}	$(6 \pm 3) \times 10^5$	(Tits et al. 2014b)
Pu(IV)	5×10^{-12}	$(2 \pm 1) \times 10^4$	(Ewart et al. 1991)
Pu(IV)*	1×10^{-8}	2×10^5	(This study)
An(IV) – Th, Np	Th: 8.5×10^{-9} Np: 1.5×10^{-10}	$(5 \pm 3) \times 10^5$	(Tits et al. 2011a)
* initial oxidation state: Pu(III)			
MO₂⁺			
Species	Initial analyte concentration c_i [mol/L]	Distribution coefficient R_d [L/kg]	source
Np(V)	1.5×10^{-10}	$\sim 5 \times 10^5$	(Tits et al. 2014b)
	1.5×10^{-10}	$3 \times 10^5 < R_d < 3 \times 10^6$	(Tits et al. 2011a)
	1×10^{-8}	5×10^5	(This study)
MO₂²⁺			
Species	Initial analyte concentration c_i [mol/L]	Distribution coefficient R_d [L/kg]	source
U(VI)	5×10^{-7}	$10^3 < R_d < 10^6$ (increasing with C:S)	(Tits et al. 2011b)
	$2 \times 10^{-10} - 3.5 \times 10^{-9}$	$3 \times 10^4 < R_d < 1.5 \times 10^5$ (increasing with C:S)	(Pointeau et al. 2004)
	1×10^{-7}	1×10^5	(This study)
Np(VI)	1.5×10^{-10}	$6 \times 10^2 < R_d < 2.5 \times 10^3$ (increasing with C:S)	(Tits et al. 2014b)
An(VI) – U, Np	Np: 1.5×10^{-10} U: 1.3×10^{-7}	$6 \times 10^2 < R_d < 10^6$ (increasing with C:S)	(Tits et al. 2011a)

4 Conclusions

The experiments performed in this study demonstrate the high retention capability of C-S-H phases towards the investigated actinides in the oxidation states from +III to +VI. All sorption experiments

showed a quantitative uptake of 98% or higher, independent of the S/L ratios in the suspensions. Also the variation of the C:S ratio did not show any significant influence on the experimental results, independent of the radionuclide and its oxidation state. These observations can be rationalized by taking into account the actinide speciation in the C-S-H suspensions, the formation of surface complexes with silanol groups of C-S-H phases and applying the concept of inter-ligand electrostatic repulsion to the uptake of actinides by C-S-H (Tits et al. 2014b).

As a positive aspect with regard to a long-term safety assessment for a radioactive waste repository, these results suggest that cement degradation, which is simulated by the variation of the C:S ratio, will have no influence on the actinides' uptake by cementitious material.

The determined average distribution coefficients R_d were about 10^5 L/kg and are in a good agreement with available literature values from $>2.7 \times 10^4$ L/kg for Eu(III) (Pointeau et al. 2001) to 1×10^6 L/kg for U(VI) (Tits et al. 2011a). The distribution coefficients for the sorption of Pu on C-S-H phases with +III as the initial oxidation state were determined to R_d values of 10^5 L/kg.

The performed HR-XANES as well as the Eh/pH measurements for the sorption samples with Pu(III) revealed a change in the oxidation state of Pu from +III to +IV during the uptake process by the C-S-H phases under alkaline conditions, independent of the applied C:S ratio.

Acknowledgments

This work was financially supported by the Federal Ministry for Economic Affairs and Energy (BMWi) under contract No. 02E11415A. Furthermore, Aerosil 300 was provided by Evonik Industries AG. The authors thank Jakob Drebert (Institute of Nuclear Chemistry, Mainz) for the XPS measurements, Regina Walter (Institute of Geosciences, Mainz) for the BET measurements and Ralf Meffert (Institute of Geosciences, Mainz) for the XRD measurements as well as Daniel Hagenlocher and Janina Stietz for their support with batch experiments.

Furthermore, the authors are grateful to two anonymous reviewers for their constructive comments that helped to improve the manuscript.

References

- Amayri, S., Fröhlich, D. R., Kaplan, U., Trautmann, N., Reich, T., 2016. Distribution coefficients for the sorption of Th, U, Np, Pu, and Am on Opalinus Clay. *Radiochim. Acta* 104, 33-40.
- Amayri, S., Jermolajev, A., Reich, T., 2011. Neptunium(V) sorption on kaolinite. *Radiochim. Acta* 99, 349-357.
- Atkins, M., Glasser, F. P., Kindness, A., 1992. Cement hydrate phases: solubility at 25°C. *Cem. Concr. Res.* 22, 241-246.
- Bahl, S., Peuge, S., Pidchenko, I., Prüßmann, T., Rothe, J., Dardenne, K., Delrieu, J., Fellhauer, D., Jegou, C., Geckeis, H., Vitova, T., 2017. Pu coexists in three oxidation states in a borosilicate glass: Implications for Pu solubility. *Inorg. Chem.* 56, 13982-13990.
- Chen, J. J., Thomas, J. J., Taylor, H. F. W., Jennings, H. M., 2004. Solubility and structure of calcium silicate hydrate. *Cem. Concr. Res.* 34, 1499-1519.
- Ewart, F. T., Glasser, F., Groves, G., Jappy, T., McCrohon, R., Moseley, P. T., Rodger, S., Richardson, I., 1991. Mechanisms of sorption in the near-field, Task 3: Characterization of radioactive waste forms - A series of final reports (1985-89) No 32C. In *nuclear science and technology*, Commission of the European Communities, *EUR 13665 EN*.
- Fanghänel, T., Neck, V., 2002. Aquatic chemistry and solubility phenomena of actinide oxides/hydroxides. *Pure Appl. Chem.* 74, 1895-1907.
- Gaona, X., Dähn, R., Tits, J., Scheinost, A. C., Wieland, E., 2011. Uptake of Np(IV) by C-S-H phases and cement paste: An EXAFS study. *Environ. Sci. Technol.* 45, 8765-8771.
- Gaona, X., Wieland, E., Tits, J., Scheinost, A. C., Dähn, R., 2013. Np(V/VI) redox chemistry in cementitious systems: XAFS investigations on the speciation under anoxic and oxidizing conditions. *Appl. Geochem.* 28, 109-118.
- Garbev, K., Beuchle, G., Bornefeld, M., Black, L., Stemmermann, P., 2008. Cell dimensions and composition of nanocrystalline calcium silicate hydrate solid solutions. Part 1: Synchrotron-based x-ray diffraction. *J. Am. Ceram. Soc.* 91, 3005-3014.
- Glasser, F. P., Lachowski, E. E., Macphee, D. E., 1987. Compositional model for calcium silicate hydrate (C-S-H) gels, their solubilities, and free-energies of formation. *J. Am. Ceram. Soc.* 70, 481-485.
- Hong, S. Y., Glasser, F. P., 1999. Alkali binding in cement pastes Part I. The C-S-H phase. *Cem. Concr. Res.* 29, 1893-1903.
- Jobmann, M., Lommerzheim, A., 2015. Projekt ANSICHT - Endlagerkonzept sowie Verfüll- und Verschlusskonzept für das Endlagerstandortmodell SÜD. DBE Technology GmbH, *TEC-26-2015-TB*.
- Kinniburgh, D. G., Cooper, D. M., 2011. PhreePlot Version 1.0: Creating graphical output with PhreeQC.
- Lommerzheim, A., Jobmann, M., 2015. Projekt ANSICHT - Endlagerkonzept sowie Verfüll- und Verschlusskonzept für das Standortmodell NORD. DBE Technology GmbH, *TEC-14-2015-TB*.

- Lothenbach, B., Nonat, A., 2015. Calcium silicate hydrates: Solid and liquid phase composition. *Cem. Concr. Res.* 78, Part A, 57-70.
- Neck, V., Kim, J. I., 2000. An electrostatic approach for the prediction of actinide complexation constants with inorganic ligands-application to carbonate complexes. *Radiochim. Acta* 88, 815-822.
- Neck, V., Kim, J. I., 2001. Solubility and hydrolysis of tetravalent actinides. *Radiochim. Acta* 89, 1-16.
- Nonat, A., 2004. The structure and stoichiometry of C-S-H. *Cem. Concr. Res.* 34, 1521-1528.
- Parkhurst, D., Appelo, C., 2016. PHREEQC (Version 3.3.5) - A computer program for speciation, batch-reaction, one-dimensional transport, and inverse geochemical calculations.
- Pidchenko, I., Kvashnina, K. O., Yokosawa, T., Finck, N., Bahl, S., Schild, D., Polly, R., Bohnert, E., Rossberg, A., Göttlicher, J., Dardenne, K., Rothe, J., Schäfer, T., Geckeis, H., Vitova, T., 2017. Uranium redox transformations after U(VI) coprecipitation with magnetite nanoparticles. *Environ. Sci. Technol.* 51, 2217-2225.
- Podkovyrina, Y., Pidchenko, I., Prübmann, T., Bahl, S., Göttlicher, J., Soldatov, A., Vitova, T., 2016. Probing covalency in the UO₃ polymorphs by U M₄ edge HR-XANES. *J. Phys.: Conf. Ser.* 712, 012092.
- Poiteau, I., Landesman, C., Giffaut, E., Reiller, P., 2004. Reproducibility of the uptake of U(VI) onto degraded cement pastes and calcium silicate hydrate phases. *Radiochim. Acta* 92, 645-650.
- Poiteau, I., Piriou, B., Fedoroff, M., Barthes, M. G., Marmier, N., Fromage, F., 2001. Sorption mechanisms of Eu(3+) on CSH phases of hydrated cements. *J. Colloid Interface Sci.* 236, 252-259.
- Ravel, B., Newville, M., 2005. ATHENA, ARTEMIS, HEPHAESTUS: data analysis for X-ray absorption spectroscopy using IFEFFIT. *J. Synchrotron Radiat.* 12, 537-541.
- Schlegel, M. L., Poiteau, I., Coreau, N., Reiller, P., 2004. Mechanism of europium retention by calcium silicate hydrates: An EXAFS study. *Environ. Sci. Technol.* 38, 4423 - 4431.
- Thoenen, T., Hummel, W., Berner, U., Curti, E., 2014. The PSI/Nagra chemical thermodynamic database 12/07. Villingen, Switzerland.
- Tits, J., Fujita, T., Harfouche, M., Dähn, R., Tsukamoto, M., Wieland, E., 2014a. Radionuclide uptake by calcium silicate hydrates: case studies with Th(IV) and U(VI). Paul Scherrer Institute, 14-03.
- Tits, J., Gaona, X., Laube, A., Wieland, E., 2011a. Influence of the redox state on the neptunium sorption by cementitious materials. In *Redox Phenomena Controlling Systems (7th EC FP CP RECOSY)*, eds. M. Altmaier, B. Kienzler, L. Duro, M. Grivé & V. Montoya, Karlsruhe Institute of Technology, 7603.
- Tits, J., Gaona, X., Laube, A., Wieland, E., 2014b. Influence of the redox state on the neptunium sorption under alkaline conditions: Batch sorption studies on titanium dioxide and calcium silicate hydrates. *Radiochim. Acta* 102, 385-400.
- Tits, J., Geipel, G., Mace, N., Eilzer, M., Wieland, E., 2011b. Determination of uranium(VI) sorbed species in calcium silicate hydrate phases: A laser-induced luminescence spectroscopy and batch sorption study. *J. Colloid Interface Sci.* 359, 248-256.

- Tits, J., Stumpf, T., Rabung, T., Wieland, E., Fanghänel, T., 2003. Uptake of Cm(III) and Eu(III) by calcium silicate hydrates: A solution chemistry and time-resolved laser fluorescence spectroscopy study. *Environ. Sci. Technol.* 37, 3568-3573.
- Tits, J., Wieland, E., Mueller, C. J., Landesman, C., Bradbury, M. H., 2006. Strontium binding by calcium silicate hydrates. *J. Colloid Interface Sci.* 300, 78-87.
- Vitova, T., Green, J. C., Denning, R. G., Löble, M., Kvashnina, K., Kas, J. J., Jorissen, K., Rehr, J. J., Malcherek, T., Denecke, M. A., 2015. Polarization dependent high energy resolution X-ray absorption study of dicesium uranyl tetrachloride. *Inorg. Chem.* 54, 174 - 182.
- Vitova, T., Pidchenko, I., Fellhauer, D., Bagus, P. S., Joly, Y., Prüßmann, T., Bahl, S., Gonzalez-Robles, E., Rothe, J., Altmaier, M., Denecke, M. A., Geckeis, H., 2017. The role of the 5f valence orbitals of early actinides in chemical bonding. *Nat. Commun.* 8, 16053.
- Zimina, A., Dardenne, K., Denecke, M. A., Doronkin, D. E., Huttel, E., Lichtenberg, H., Mangold, S., Prüßmann, T., Rothe, J., Spangenberg, T., Steininger, R., Vitova, T., Geckeis, H., Grunwaldt, J. D., 2017. CAT-ACT - A new highly versatile X-ray spectroscopy beamline for catalysis and radionuclide science at the KIT synchrotron light facility ANKA. *Rev. Sci. Instrum.* 88, 113113.
- Zimina, A., Dardenne, K., Denecke, M. A., Grunwaldt, J. D., Huttel, E., Lichtenberg, H., Mangold, S., Prüßmann, T., Rothe, J., Steininger, R., Vitova, T., 2016. The CAT-ACT Beamline at ANKA: A new high energy X-ray spectroscopy facility for CATalysis and ACTinide research. *J. Phys. Conf. Ser.* 712, 012019.

Figure and Table legends

- Figure 1: Measured pH values in C-S-H suspensions (0.5 – 20.0 g/L) in MilliQ water after two weeks of synthesis of C-S-H phases with different C:S ratios. 10
- Figure 2: Composition of the aqueous solution after equilibration with C-S-H phases with different C:S ratios in MilliQ water (S/L = 15 g/L) determined by ICP-MS and comparison to literature data. 11
- Figure 3: Distribution coefficients R_d for the sorption of Am(III), Th(IV), Np(V) and U(VI) on C-S-H phases with C:S 0.75 (C:S 1.07 for Np(V)) in MilliQ water as a function of S/L ratios between 0.7 – 19.0 g/L. The dotted line corresponds to R_d values calculated for an actinide uptake of 99%. 14
- Figure 4: Distribution coefficients R_d for the sorption of Pu(III), Am(III), Th(IV), Np(V) and U(VI) on C-S-H phases in MilliQ water for S/L = 5.0 g/L and C:S ratios between 0.7 – 1.8. The dotted line corresponds to R_d values calculated for an actinide uptake of 99%. 15
- Figure 5: Predominance diagram for an equilibrium concentration of 1×10^{-9} M U(VI) in the system C-S-H/MilliQ water for C:S ratios of 0.75, 1.07 and 1.65. The grey dots mark the measured Eh and pH values of the sorption samples. (Graphic generated by PhreePlot (version 1.0, (Kinniburgh and Cooper 2011)) using PHREEQC and the PSI database (Nagra 12/07)). 18
- Figure 6: Predominance diagram for an equilibrium concentration of 1×10^{-10} M Np(V) in the system C-S-H/ MilliQ water for C:S ratios between 0.75 – 1.65. The grey dots mark the measured Eh and pH values of sorption samples with different C:S ratios. (Graphics generated by PhreePlot (version 1.0, (Kinniburgh and Cooper 2011)) using PHREEQC and the PSI database (Nagra 12/07)). 19
- Figure 7: Predominance diagram for an equilibrium concentration of 1×10^{-10} M Pu(III) in the system C-S-H/ MilliQ water for C:S ratios between 0.7 – 1.8. The grey dots mark the measured Eh and pH values of the sorption samples with different C:S ratios and the samples for HR-XANES with C:S 0.75 and 1.65. (Graphics generated by PhreePlot (version 1.0, (Kinniburgh and Cooper 2011)) using PHREEQC and the PSI database (Nagra 12/07)). 20
- Figure 8: Pu M_5 edge HR-XANES spectra of the Pu/C-S-H samples with C:S 0.75 and C:S 1.65 and the corresponding Pu(IV)O₂ reference. 21
- Table 1: Concentration of calcium and silicon in the supernatant solution of C-S-H phases with S/L = 15.0 g/L and V = 40 mL determined by ICP-MS measurements and calculated C:S ratio. 12
- Table 2: C:S target ratios in comparison to the C:S ratios determined by XPS measurements (the estimated errors are about $\pm 10\%$) and literature data. 13
- Table 3: Peak maxima for the Pu(III)³⁺, Pu(IV)O₂ and Pu(VI)O₂²⁺ oxidation state references (white line and post edge feature) (Bahl et al. 2017) and for the studied samples. 21
- Table 4: Comparison of the results of this study (average distribution coefficients $R_{d(av)}$) for all samples of one species independent of S/L and C:S ratio) with available literature data for distribution coefficients of different metal cations in the oxidation states from +III to +VI. 23

Figures:

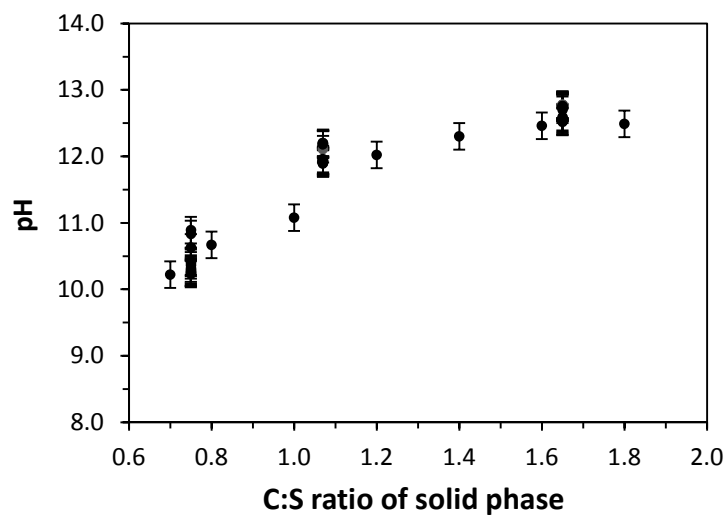


Figure 1: Measured pH values in C-S-H suspensions (0.5 – 20.0 g/L) in MilliQ water after two weeks of synthesis of C-S-H phases with different C:S ratios.

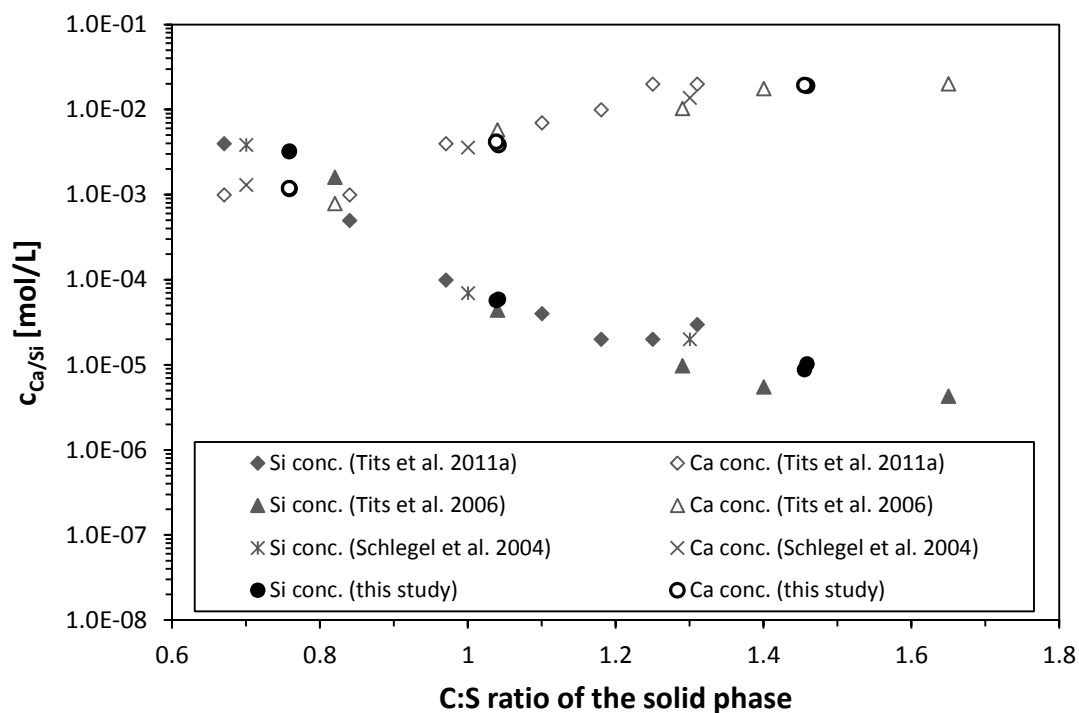


Figure 2: Composition of the aqueous solution after equilibration with C-S-H phases with different C:S ratios in MilliQ water ($S/L = 15$ g/L) determined by ICP-MS and comparison to literature data.

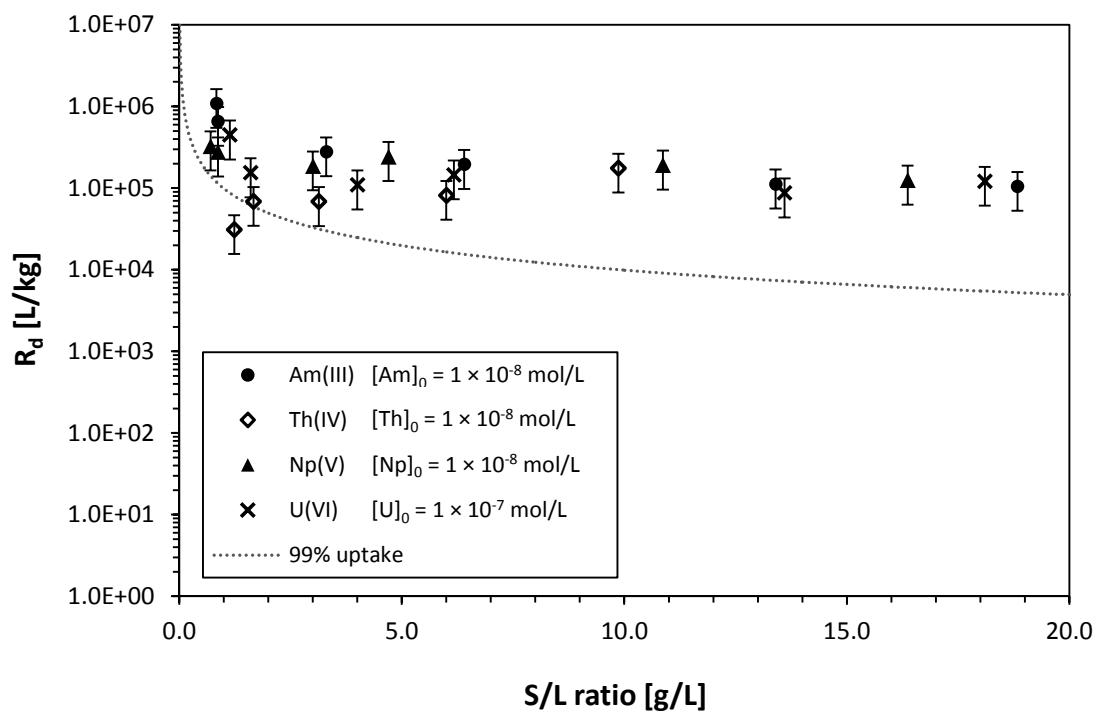


Figure 3: Distribution coefficients R_d for the sorption of Am(III), Th(IV), Np(V) and U(VI) on C-S-H phases with C:S 0.75 (C:S 1.07 for Np(V)) in MilliQ water as a function of S/L ratios between 0.7 – 19.0 g/L. The dotted line corresponds to R_d values calculated for an actinide uptake of 99%.

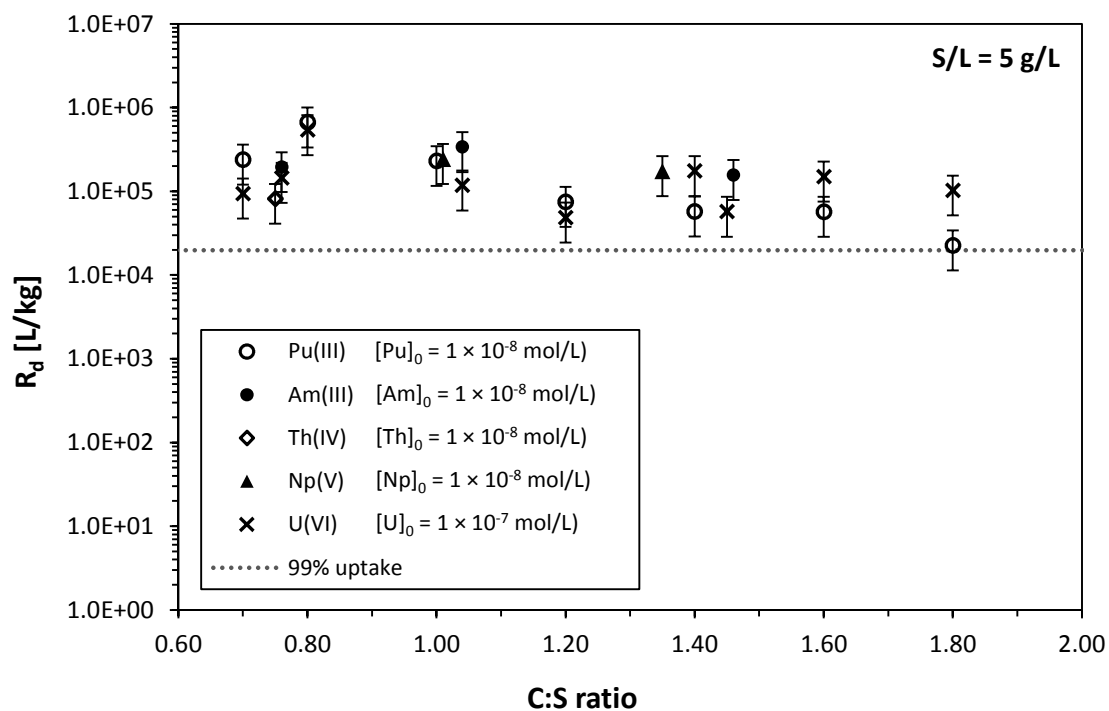


Figure 4: Distribution coefficients R_d for the sorption of Pu(III), Am(III), Th(IV), Np(V) and U(VI) on C-S-H phases in MilliQ water for S/L = 5.0 g/L and C:S ratios between 0.7 – 1.8. The dotted line corresponds to R_d values calculated for an actinide uptake of 99%.

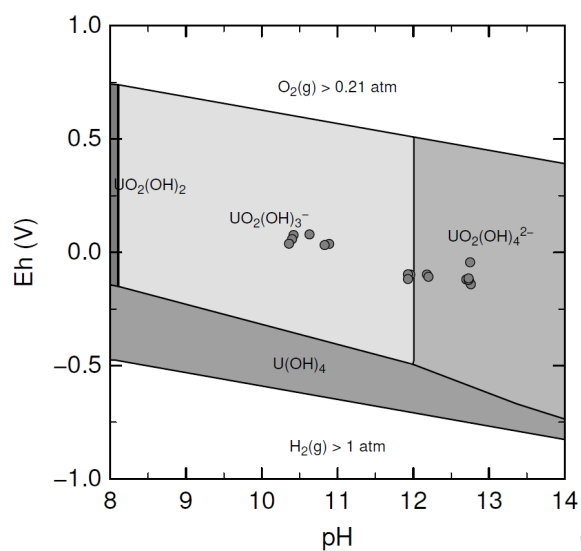


Figure 5: Predominance diagram for an equilibrium concentration of 1×10^{-9} M U(VI) in the system C-S-H/MilliQ water for C:S ratios of 0.75, 1.07 and 1.65. The grey dots mark the measured Eh and pH values of the sorption samples. (Graphic generated by PhreePlot (version 1.0, (Kinniburgh and Cooper 2011)) using PHREEQC and the PSI database (Nagra 12/07)).

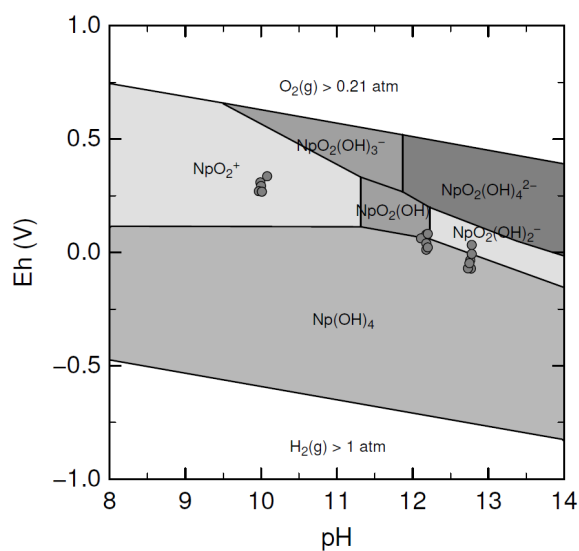


Figure 6: Predominance diagram for an equilibrium concentration of $1 \times 10^{-10} \text{ M Np(V)}$ in the system C-S-H/ MilliQ water for C:S ratios between 0.75 – 1.65. The grey dots mark the measured Eh and pH values of sorption samples with different C:S ratios. (Graphics generated by PhreePlot (version 1.0, (Kinniburgh and Cooper 2011)) using PHREEQC and the PSI database (Nagra 12/07)).

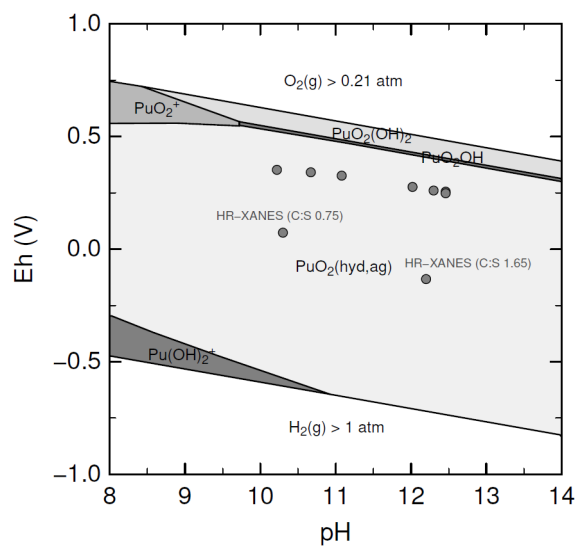


Figure 7: Predominance diagram for an equilibrium concentration of $1 \times 10^{-10} \text{ M Pu(III)}$ in the system C-S-H/ MilliQ water for C:S ratios between 0.7 – 1.8. The grey dots mark the measured Eh and pH values of the sorption samples with different C:S ratios and the samples for HR-XANES with C:S 0.75 and 1.65. (Graphics generated by PhreePlot (version 1.0, (Kinniburgh and Cooper 2011)) using PHREEQC and the PSI database (Nagra 12/07)).

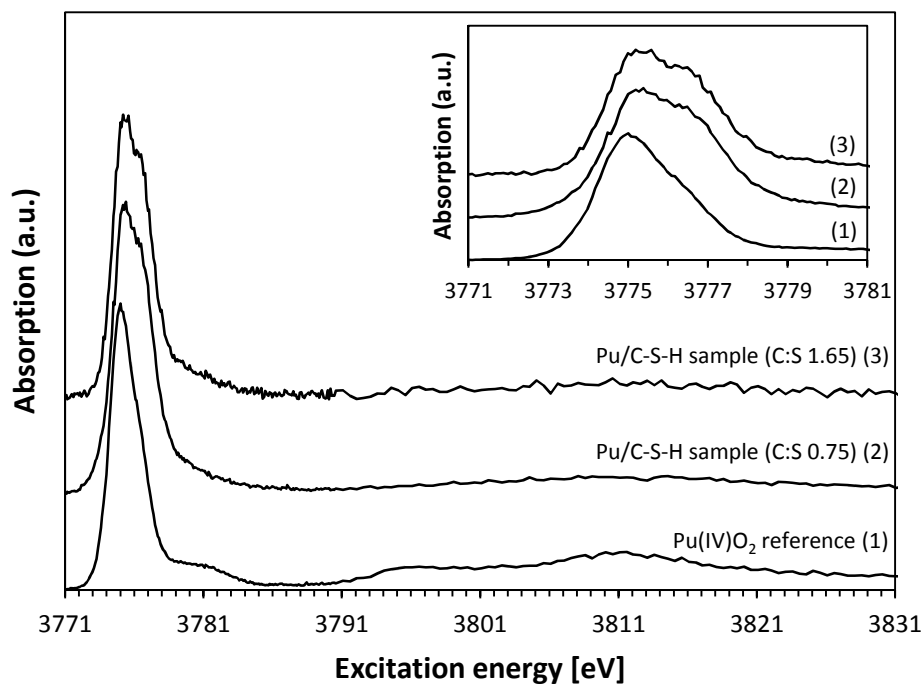


Figure 8: Pu M_5 edge HR-XANES spectra of the Pu/C-S-H samples with C:S 0.75 and C:S 1.65 and the corresponding Pu(IV)O₂ reference.

*Tables:**Table 1: Concentration of calcium and silicon in the supernatant solution of C-S-H phases with S/L = 15.0 g/L and**V = 40 mL determined by ICP-MS measurements and calculated C:S ratio.*

C:S target ratio	$n_i(\text{Ca})^*$ [mol]	$n_i(\text{Si})^*$ [mol]	$c_{\text{sol.}}(\text{Ca})$ [mol/L]	$c_{\text{sol.}}(\text{Si})$ [mol/L]	calculated C:S ratio of the solid phase
0.75	4.41×10^{-3}	5.87×10^{-3}	$(1.2 \pm 0.2) \times 10^{-3}$	$(3.2 \pm 1.0) \times 10^{-3}$	0.76
1.07	5.35×10^{-3}	5.00×10^{-3}	$(4.0 \pm 0.2) \times 10^{-3}$	$(5.8 \pm 1.9) \times 10^{-5}$	1.04
1.65	6.49×10^{-3}	3.93×10^{-3}	$(1.9 \pm 0.1) \times 10^{-2}$	$(9.6 \pm 3.5) \times 10^{-6}$	1.46

* Moles used in synthesis

Table 2: C:S target ratios in comparison to the C:S ratios determined by XPS measurements (the estimated errors are about $\pm 10\%$) and literature data.

C:S target ratio	0.70	0.75	1.20	1.80
C:S ratio (XPS)	0.63	0.70	0.98	1.25
C:S (Tits et al. 2006) bulk analysis (ICP-OES)	-	0.82	-	1.65*

* For a C:S target ratio of 1.82

Table 3: Peak maxima for the Pu(III)(aq), Pu(IV)O₂ and Pu(VI)O₂²⁺ oxidation state references (white line and post edge feature) (Bahl et al. 2017) and for the studied samples.

White line of Pu M ₅ edge HR-XANES	Energy / eV
Pu(III)(aq)	3774.1*
Pu(IV)O ₂	3775.0*
Pu(VI)O ₂ ²⁺	3776.2*
Post edge feature of Pu(VI)O ₂ ²⁺	3780.5*
Pu/C-S-H sample (C:S 0.75)	3775.4*
Pu/C-S-H sample (C:S 1.65)	3775.2*

* The spectra are measured without slit in front of the sample.

Table 4: Comparison of the results of this study (average distribution coefficients $R_d(av)$ for all samples of one species independent of S/L and C:S ratio) with available literature data for distribution coefficients of different metal cations in the oxidation states from +III to +VI.

M³⁺			
Species	Initial analyte concentration c_i [mol/L]	Distribution coefficient R_d [L/kg]	source
Eu(III)	1×10^{-4}	$\geq 2.7 \times 10^4$	(Pointeau et al. 2001)
	2.6×10^{-10}	$\geq 1.8 \times 10^5$	
Am(III)	2×10^{-9}	$(6 \pm 3) \times 10^5$	(Tits et al. 2003)
	1×10^{-11}	$(6 \pm 2) \times 10^4$	(Ewart et al. 1991)
	1×10^{-8}	4×10^5	(This study)
M⁴⁺			
Species	Initial analyte concentration c_i [mol/L]	Distribution coefficient R_d [L/kg]	source
Th(IV)	1×10^{-8}	2×10^5	(This study)
Np(IV)	1.5×10^{-10}	$(6 \pm 3) \times 10^5$	(Tits et al. 2014b)
Pu(IV)	5×10^{-12}	$(2 \pm 1) \times 10^4$	(Ewart et al. 1991)
Pu(IV)*	1×10^{-8}	2×10^5	(This study)
An(IV) – Th, Np	Th: 8.5×10^{-9} Np: 1.5×10^{-10}	$(5 \pm 3) \times 10^5$	(Tits et al. 2011a)
* initial oxidation state: Pu(III)			
MO₂⁺			
Species	Initial analyte concentration c_i [mol/L]	Distribution coefficient R_d [L/kg]	source
Np(V)	1.5×10^{-10}	$\sim 5 \times 10^5$	(Tits et al. 2014b)
	1.5×10^{-10}	$3 \times 10^5 < R_d < 3 \times 10^6$	(Tits et al. 2011a)
	1×10^{-8}	5×10^5	(This study)
MO₂²⁺			
Species	Initial analyte concentration c_i [mol/L]	Distribution coefficient R_d [L/kg]	source
U(VI)	5×10^{-7}	$10^3 < R_d < 10^6$ (increasing with C:S)	(Tits et al. 2011b)
	$2 \times 10^{-10} - 3.5 \times 10^{-9}$	$3 \times 10^4 < R_d < 1.5 \times 10^5$ (increasing with C:S)	(Pointeau et al. 2004)
	1×10^{-7}	1×10^5	(This study)
Np(VI)	1.5×10^{-10}	$6 \times 10^2 < R_d < 2.5 \times 10^3$ (increasing with C:S)	(Tits et al. 2014b)
An(VI) – U, Np	Np: 1.5×10^{-10} U: 1.3×10^{-7}	$6 \times 10^2 < R_d < 10^6$ (increasing with C:S)	(Tits et al. 2011a)

Highlights – Uptake of Actinides by Calcium Silicate Hydrate (C-S-H) Phases

- First investigation of Pu uptake by C-S-H phases combining batch experiments with Pu M₅-edge high-resolution XANES spectroscopy
- Similar R_d values determined for Am(III), Pu(III), Th(IV), Np(V) and U(VI), independent of the C:S (0.7-1.8) and S/L (0.5-20 g/L) ratios
- XPS measurements indicate a depletion of Ca at the surface of the C-S-H phases